Electron localization in amorphous solids: numerical studies for the distorted diamond lattice

1992 J. Phys.: Condens. Matter 4 6109

(http://iopscience.iop.org/0953-8984/4/28/011)

J. Phys.: Condens. Matter 4 (1992) 6109–6118. Printed in the UK

Electron localization in amorphous solids: numerical studies for the distorted diamond lattice

Th Koslowski and W von Niessen

Institut für Physikalische und Theoretische Chemie, Technische Universität Braunschweig, Hans-Sommer-Straße 10, D-3300 Braunschweig, Federal Republic of Germany

Received 10 February 1992, in final form 22 April 1992

Abstract. We present a numerical study of localization properties on models for amorphous solids in three dimensions. Tight-binding Hamiltonians that are based on the diamond structure are used to describe the electronic structure of amorphous modifications of carbon, silicon and germanium. The localization behaviour of electronic states is calculated by studying the sensitivity of eigenvalues to a change in boundary conditions. A wide spectrum of localization effects can be observed, including electron localization both at the band edges and weak localization within the bands. The origin of electron localization is discussed using a population analysis of eigenfunctions.

1. Introduction

In the study of covalently bonded amorphous semiconductors, continuous random networks (CRNs) are a widely used model for constructing the geometry of these systems. In a CRN, all atoms retain their normal coordination number $Z = 4$, and deviations from crystalline bond lengths and bond angles are small (Polk 1971). However, the translational invariance of the perfect lattice is destroyed and disorder is introduced. From a fundamental theorem of Anderson (1958), all eigenfunctions of a disordered system become localized if the strength of the disorder exceeds some critical value. For a given disorder smaller than this critical value, the density of states can be divided into a part where all states are localized and another part containing extended states, separated by a mobility edge E_c (Ziman 1969, Mott and Davis 1971). As charge transport starting from a localized state can only be performed by phonon-assisted hopping or by exciting an electron into the part of the spectrum that contains extended states, the conductivity of the system can be affected drastically by electron localization. Thus, in addition to the knowledge of the density of states, the localization behaviour of eigenfunctions is of particular interest in the study of any disordered system.

The electronic structure of CRNs modelling amorphous silicon has attracted considerable interest in recent numerical work. Two different types of CRNs have been used by Nichols and Winer (1988) to calculate the localization behaviour of band-edge states in amorphous silicon. Biswas *et al* (1989) have studied the density of states of both a perfect CRN and a CRN including dangling bonds. The local density of states of certain defects in amorphous silicon (a-Si) has been obtained by Agrawal *et al* (1990) on a Bethe lattice. All of these calculations are based on a tight-binding

0953-8984/92/286109+10$04.50

Hamiltonian; the wavefunctions are constructed as linear combinations of atomic orbitals. Using the Bloch functions of the crystal as basis functions Hickey and Morgan (1986) obtained the density of states and a measure of the broadening of functions in k-space, related to the lifetime of Bloch functions in an amorphous system.

The calculations presented in this article are an application of the approach developed by the present authors (Koslowski and von Niessen 1992) to calculate the localization properties of eigenfunctions of CRNs in two dimensions. The role of the presence of odd-membered rings and bond-angle disorder will be studied using a nearest-neighbour tight-binding Hamiltonian including s- and p-type orbitals as basis functions. The influence of bond-length variation will be studied by a $1/r^2$-scaling of the Hamiltonian matrix elements. All CRNs are relaxed by a Monte Carlo method. The construction of the network, the Hamiltonian parameters and the way localization properties are calculated will be presented in the next section. Results are presented and discussed in section 3. A detailed study of localization properties, depending on atomic number, parametrization and the degree of disorder will be given there. The origin of localization will be analysed using an orbital population analysis. Conclusions are derived in the last section.

2. Methods

Out of the numerous ways to construct a CRN based on the diamond lattice, we have chosen the vacancy model of Duffy *et al* (1974). It provides a fast computational generation, the use of cyclic boundary conditions and the absence of dangling bonds. Excluding hand-built models, these requirements may also be fulfilled by the models of Henderson and Herman (1972), Connel and Temkin (1974) or the W3 model (Wooten *et al* 1985). The vacancy model has been chosen because it provides a simple measure for the degree of disorder introduced to the system. Geometries arising from a molecular-dynamics simulation (Biswas *et al* 1987) include three- and five-coordinated silicon atoms and thus do not represent a CRN. Details of the construction of a CRN by a vacancy model are given by Duffy *et al* (1974). As in the CRN construction on the square lattice (Koslowski and von Niessen 1992), double bonds are avoided by restricting the elimination of atoms to four out of eight atoms in an elementary cell. Their positions are $(\frac{1}{4},\frac{1}{4},\frac{1}{4})$, $(\frac{3}{4},\frac{3}{4},\frac{1}{4})$, $(\frac{1}{4},\frac{3}{4},\frac{3}{4})$ and $(\frac{3}{4},\frac{1}{4},\frac{3}{4})$. There are three possibilities to create two new bonds connecting the four atoms around each vacancy, which are chosen at random with equal probability. In addition to the six-membered rings present in the diamond lattice, five-membered rings are created on a CRN. The degree of disorder introduced to the network is measured by the vacancy concentration p. In our notation, p is normalized to the number of all possible vacancies, i.e. half of the atoms. To get the actual vacancy concentration referring to all atoms, p has to be divided by two.

The large distortions in bond lengths and bond angles generated by the vacancy model have to be removed by the relaxation of the lattice. For this relaxation, the Keating potential

$$U_i = \frac{3\alpha}{16R_0^2}\sum_{i\neq j}(R_{ij}^2 - R_0^2)^2 + \frac{3\beta}{8R_0^2}\sum_{i(j,k)}(R_{ji}\cdot R_{ki} + \tfrac{1}{3}R_0^2)^2 \qquad (1)$$

is used (Keating 1966). R_{ij} is the distance vector between two neighbour atoms. The second sum spans all distinct pairs of neighbours of i. The first term in equation (1)

corresponds to an atom–atom interaction, the second term describes a bond–bond interaction. For Si and Ge, the Keating parameters give $\alpha/\beta = 3.5$. For carbon, the ratio α/β is 1.5, so bond–bond interactions become more important there. Whereas pair distribution functions similar to those of CRNs can be observed for amorphous films of Si and Ge, amorphous carbon is believed to be polycrystalline. Anyway, a comparison of the localization properties of carbon with those of silicon and germanium is interesting, because the influence of a different geometry and different sets of tight-binding parameters can be studied. A Monte Carlo method is used to look for the potential energy minimum. For a system containing n atoms, $2n$ Monte Carlo steps have been performed. On average, the attempt to move an atom is made once for every Monte Carlo step. The maximum displacement in each direction has been set to $R_0/10$, the attempt to move an atom has only been put into effect if it has caused a decrease in energy.

A simple nearest-neighbour tight-binding Hamiltonian

$$\hat{H} = \sum_{ia} \epsilon_{ia} \hat{c}_{ia}^{+} \hat{c}_{ia} + \sum_{i \neq j, a, b} V_{iajb} \hat{c}_{ia}^{+} \hat{c}_{jb} \tag{2}$$

is used to calculate the electronic structure of the CRN. $\hat{c}_{ia}$ and $\hat{c}_{ia}^{+}$ are annihilation and creation operators operating on the space of valence atomic orbitals localized at sites i. To make a distinction between the four different types of orbitals attached to each atom, the indices a and b have been introduced. The complete set of atomic orbitals is assumed to be orthonormal. For all elements mentioned above, the parameters of Chadi and Cohen (1975) have been used. No dependence of V_{iajb} on the interatomic distance has been imposed here. In addition to the presence of odd-membered rings, the variation of bond angles causes disorder in the direction cosines, leading to disorder in the off-diagonal matrix elements. For carbon and silicon, matrix element scaling of the type

$$V_{iajb}(r) = V_{iajb}(R_0) R_0^2 / r^2 \tag{3}$$

in addition to the other calculations has been used. This scaling is due to Harrison (1980), whose parameter sets have been used. All energies are given in eV; as the zero of energy the valence orbital ionization potential ϵ_s of the corresponding s orbital has been chosen.

To study the localization properties of the elements in their amorphous modification, we use the method of Thouless, Edwards and Licciardello (Edwards and Thouless 1972, Licciardello and Thouless 1975, 1978), abbreviated to TEL, in combination with a scaling principle. The authors mentioned above were able to show that the energy shift ΔE caused by a change in boundary conditions is related to the conductance of a system with length L by

$$G(L) = \frac{e^2}{2\hbar} \frac{\Delta E(L)}{\delta E(L)}. \tag{4}$$

δE is the average spacing of the energy levels. In practice, ΔE and δE are averages within an energy interval. Due to its large fluctuations, ΔE is usually taken as a geometric mean. In the original TEL work, boundary conditions have been changed from cyclic to anticyclic ones. To avoid eigenvalue crossings, which usually

lead to difficulties in the analysis of data within the framework of the TEL method, the weak decoupling TEL scheme (Koslowski and von Niessen 1992) is used in this work. For each realization, eigenvalues are calculated for cyclic boundary conditions and modified cyclic boundary conditions in one direction. For modified cyclic boundary conditions, matrix elements that connect atomic orbitals on opposite lattice sides are multiplied by a factor 0.99. The Thouless number $g(L) = \Delta E(L)/\delta E(L)$ obtained this way differs from the number obtained from the strong coupling case only by a constant factor, which does not affect the calculation of the localization behaviour. Energy-resolved Thouless numbers are calculated for different system sizes L. Whenever $g(L)$ increases with increasing lattice size, the corresponding eigenstates are extended. If $g(L)$ decreases with increasing lattice size, the corresponding eigenstates are localized. This interpretation is in agreement with the scaling theory of localization (Abrahams *et al* 1979), where the sign of the scaling function $\beta = \mathrm{d}\ln g(L)/\mathrm{d}\ln L$ is used to classify the localization character of eigenfunctions. It should be noted that the scaling method used in the present article is independent of the existence of a one-parameter scaling function $\beta(g)$, as postulated in the scaling theory of localization. To calculate the eigenvalues of the large sparse matrices arising from equation (2), a Lanczos algorithm (Lanczos 1950, Cullum and Willoughby 1985) has been used. The main advantage of the TEL approach is that only two sets of eigenvalues are required to distinguish localized from extended states. For sparse matrices like those arising from the tight-binding approximation (2), the calculation of eigenvalues is much cheaper than the calculation of eigenvectors, considering both computer time and storage. For the population analysis presented in the third section, eigenvectors are required. They are computed for a small system, using just a single realization. For the calculation of the scaling behaviour of localization measures based on eigenfunctions like the inverse participation ratio (Dean and Bell 1970), larger systems would have to be studied with a large number of realizations.

3. Results and discussion

Localization on CRNs using Hamiltonian matrix elements independent of the interatomic distance has been studied for a-C, a-Si and a-Ge with vacancy concentrations of $p = 0.1$, $p = 0.2$, $p = 0.4$ and $p = 0.8$. In addition, for a-C and a-Si $1/r^2$-scaling of the matrix elements has been studied at $p = 0.05$, $p = 0.1$ and $p = 0.2$. Calculations have been performed on systems with linear dimensions $L = 3$, $L = 4$ and $L = 5$, where L denotes the length of an elementary cell. An elementary cell contains eight atoms or 32 atomic orbitals. For the smallest vacancy concentrations ($p = 0.05$), eigenvalue problems of dimensions about 3900 (975 atoms) had to be solved for $L = 5$. Referring to all elements and to all degrees of disorder, the minimum number of realizations used are 134 ($L = 3$), 23 ($L = 4$) and 5 ($L = 5$). The maximum number of realizations used are 366 ($L = 3$), 65 ($L = 4$) and 13 ($L = 5$). Looking at the comparison of radial distribution functions obtained from experiments and from the vacancy model (Duffy *et al* 1974), the best representation of the experimental radial distribution function can be obtained around $p = 0.06$.

The TEL analysis can be explained with the help of figure 1(*a*). The energy interval [−10 eV, 20 eV] has been divided into 64 subintervals. Of these subintervals, 46 show a non-zero density of states for all system lengths. Within each subinterval, the behaviour of the negative decadic logarithm of the Thouless number, $-\log_{10} g$, with

increasing lattice size is plotted from the left. If $-\log_{10} g$ is increasing with increasing lattice size, the corresponding eigenstates are localized and the energy bin is marked with an L. In the density of states plot figure 1(*b*), energy intervals containing localized states have been shaded. It should be noted that the calculations presented in this article are less accurate than those for two-dimensional CRNs (Koslowski and von Niessen 1992). In the two-dimensional case, L ranges from 20 to 50 with a step size of ten, so a larger length scale has been used to study the scaling behaviour of the Thouless number there. As only three system lengths are used to analyse the localization behaviour of eigenfunctions in the three-dimensional problem, we have refrained from computing any quantitative measure of electron localization like the localization length. The localization length L_{loc} is a measure for the spatial extension of a localized eigenfunction. Assuming an exponential behaviour of the conductance for localized states

$$g(L) \propto \exp(-L/L_{\mathrm{loc}}) \tag{5}$$

the localization length can in principle be computed from a least-squares fit. Although the quality of the data is not sufficient to perform such an analysis, a qualitative comparison of the strength of localization can be obtained by an inspection of the TEL plots. The density of states (DOS) shown in the figures is accumulated from all systems, regardless of L.

Using $1/r^2$-scaling of the Hamiltonian matrix elements, the localization behaviour of the eigenfunctions of a-Si is as follows. At $p = 0.05$ (figure 1), localized eigenfunctions can be observed in a small interval at the bottom of the conduction band (CB) and in a larger interval at the top of the conduction band. Whereas the density of states in the localized region at the bottom of the CB is small, localization at the top of the CB persists down to an energy showing the largest DOS of the entire spectrum. The valence band (VB) shows no localized states at all. The density of states of the CB and the VB shows a well-defined structure, including the three well-known peaks in the valence band DOS that can be observed in photoelectron spectra of crystalline silicon. Photoelectron spectra obtained from films of a-Si are structureless, unlike the valence band DOS obtained in our computations. However, phonon broadening may hide this structure in experiments. The valence band DOS obtained by Biswas *et al* (1987) and Nichols and Winer (1988) shows two peaks. However, both spectra have been broadened. In addition to localization in the CB, at $p = 0.1$ (figure 2) localization at the top of the VB can be observed. States at the bottom of the CB are more localized, i.e. have a smaller localization length, and the energy interval showing localized eigenfunctions is larger. At $p = 0.2$ (figure 3), the band gap at the Fermi energy is closed, although the DOS is still small here. No TEL analysis has been performed in the interval showing the smallest DOS at $E = 5.5$ eV, because the DOS for the realizations performed at $L = 5$ was zero. Localization at the top of the VB is reduced to a region with a small DOS. The conduction band DOS has become structureless, in the valence band DOS the two rightmost peaks have almost merged. The most important points in the analysis performed in this and the following paragraphs are collected in table 1. In figures 1 and 2, the Fermi energy is located in the band gap. In figure 3, E_{F} is located in the interval around $E = 5$ eV that shows the smallest DOS.

Let us summarize the results obtained for a-Si without the $1/r^2$-scaling of the matrix elements. At $p = 0.1$, the localization behaviour around E_{F} remains unchanged. At the bottom of the VB, localization can be observed. The most striking

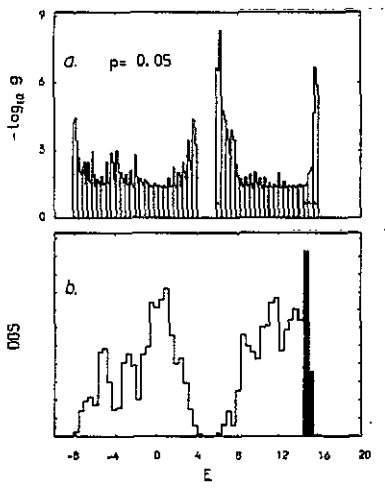

Figure 1. TEL analysis (*a*) and density of states (*b*) for a-Si, $1/r^2$-scaling, vacancy concentration $p = 0.05$. Energy in units of eV.

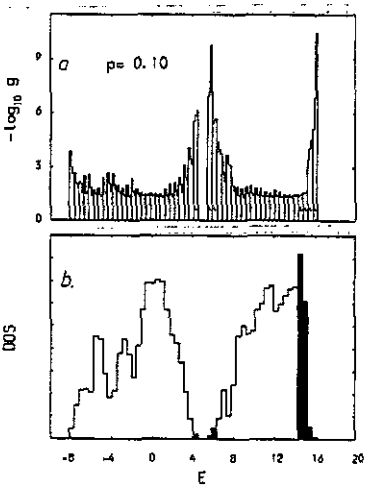

Figure 2. TEL analysis (*a*) and density of states (*b*) for a-Si, $1/r^2$-scaling, vacancy concentration $p = 0.10$. Energy in units of eV.

Table 1. A collection of localization properties and DOS features. $1/r^2$ denotes r-dependent Hamiltonian matrix elements according to equation (3).

System	p	DOS at E_F	Localization at E_F	Inner-band localization	No of VB DOS peaks
C	0.10	Zero	CB	CB	3
	0.20	Zero	VB	CB	2
	0.40	Small	yes	CB	2
	0.80	High	no	no	—
C, $1/r^2$	0.05	Zero	VB, CB	VB, CB	2–3
	0.10	Zero	VB, CB	VB, CB	—
	0.20	Zero	VB, CB	No	—
Si	0.10	Zero	VB, CB	CB	2–3
	0.20	Zero	VB	CB	2
	0.40	Small	Yes	No	2
	0.80	High	No	No	—
Si, $1/r^2$	0.05	Zero	CB	No	3
	0.10	Zero	VB, CB	No	3
	0.20	Small	Yes	No	2–3
Ge	0.10	Zero	No	No	3
	0.20	Small	Yes	No	2–3
	0.40	High	No	No	2
	0.80	High	No	No	—

difference to the distance-dependent Hamiltonian can be observed at the top of the CB. In addition to localization at the band edge, localized eigenfunctions can also be observed in the interior of the band, separated from the localized states at the

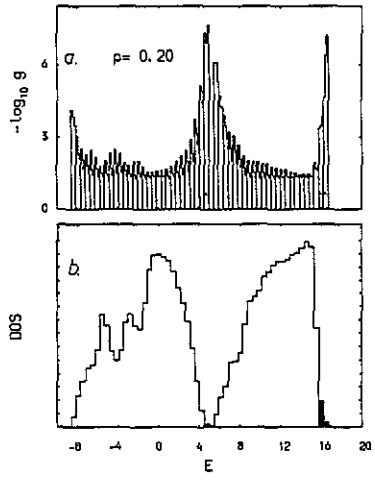

Figure 3. TEL analysis (*a*) and density of states (*b*) for a-Si, $1/r^2$-scaling, vacancy concentration $p = 0.20$. Energy in units of eV.

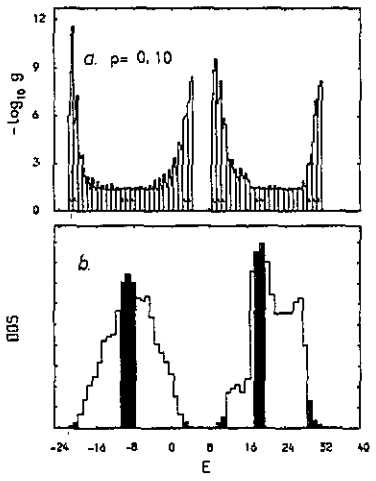

Figure 4. TEL analysis (*a*) and density of states (*b*) for a-C, $1/r^2$-scaling, vacancy concentration $p = 0.10$. Energy in units of eV.

band edge by a region of extended states. This inner-band localization persists up to $p = 0.2$. As this phenomenon is even more pronounced for amorphous carbon, it will be illustrated there. At $p = 0.2$ and $p = 0.4$, the structure in the conduction band DOS has disappeared, the valence band DOS is smooth and shows two peaks. At $p = 0.4$, the gap at E_F has closed and only a small interval at E_F shows a localized behaviour. The DOS is broad and structureless at $p = 0.8$, a small valley has replaced the gap between the valence and conduction band. Localization can only be observed in a small region at the top of the CB and at the bottom of the VB.

For a-Ge, the localization behaviour and the DOS structure can be described as follows. At $p = 0.1$, localization can be observed at the top of the CB and at the bottom of the VB. Inner-band localization occurs in the conduction band, it disappears at higher values of p. Although the DOS at E_F equals zero, no localization shows up there. The gap at E_F closes at $p = 0.2$, the DOS is small there and a small interval of localized states exists. The gap is filled considerably at $p = 0.4$, until it becomes equal to the DOS in the interior of the VB and the CB at $p = 0.8$. At $p = 0.4$ and $p = 0.8$, there is no localization except at the bottom of the VB and at the top of the CB.

For small vacancy concentrations ($p = 0.05$ and $p = 0.1$), a-C ($1/r^2$-scaling) shows inner-band localization in the CB and in the VB in addition to localization at the top and bottom of the VB and CB. This behaviour is illustrated in figure 4. It should be noted that this inner-band localization is much weaker than the localization that can be observed at all band edges. As for a-Si ($1/r^2$-scaling), electron localization at the bottom of the CB is stronger than localization at the top of the VB. At $p = 0.2$, the bands are still separated but the DOS has become featureless in both bands. The Fermi energy is located in the gap.

Using distance-independent Hamiltonian matrix elements for a-C the phenomenon of weak inner-band localization can only be observed in the conduction band up to $p = 0.4$. As for a-Si with a comparable Hamiltonian, the localization

behaviour around E_F is somewhat irritating. States are localized at the bottom of the CB at $p = 0.1$, whereas states at the top of the VB are extended. At $p = 0.2$, the situation is reversed. Unlike their $1/r^2$-scaling counterparts, the TEL data around E_F are not unambiguous, so the question about the localization behaviour at this energy remains unanswered. At $p = 0.4$, the gap at E_F has closed, states within the gap are clearly localized. At $p = 0.8$, the gap has filled up considerably, states in the gap have become extended.

Looking at electron localization around the Fermi energy for the r-dependent Hamiltonians, it can be concluded that localization is stronger at the bottom of the CB than at the top of the VB. An extreme case can be observed for a-Si at $p = 0.05$, where states at the top of the VB are extended. That states at the bottom of the CB are more localized than at the top of the VB has also been observed by Nichols and Winer (1988) studying small realizations of three different CRN models (216 atoms, one realization and 54 atoms, two realizations). However, they have not been able to distinguish localized from extended states.

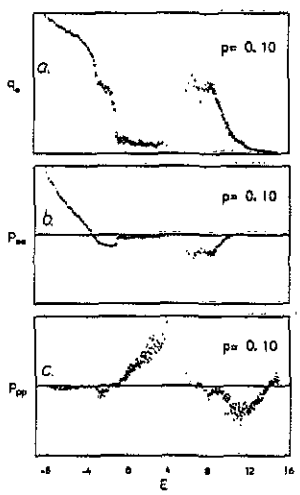

Figure 5. Population analysis for a-Si, vacancy concentration $p = 0.10$, $1/r^2$-scaling. (*a*) s-type charge order, (*b*) ss bond order and (*c*) ppσ bond order. Energy in units of eV.

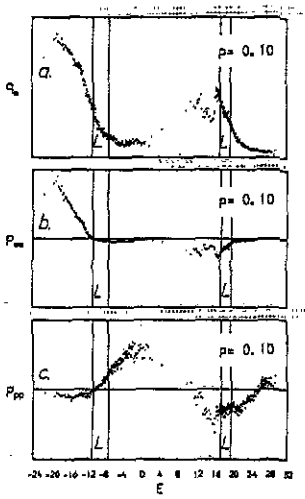

Figure 6. Population analysis for a-C, vacancy concentration $p = 0.10$, $1/r^2$-scaling. (*a*) s-type charge order, (*b*) ss bond order and (*c*) ppσ bond order. Energy in units of eV. Energy intervals containing weakly localized states are marked with an L.

To explain the asymmetry in the localization behaviour around E_F, we have performed a population analysis (Mulliken 1955). For a-Si (p=0.1, $1/r^2$-scaling), the charge order resulting from s-type orbitals, i.e. the projection of an eigenfunction onto the space of s-type orbitals is plotted in figure 5. In addition, the ss bond order and the pp bond order are given. The charge order q_s^α corresponding to the eigenstate $|\alpha\rangle$ is given by

$$q_s^\alpha = \sum_i \langle\alpha|i\rangle\langle i|\alpha\rangle \tag{6}$$

where the summation is restricted to s-type basis functions. The bond orders are given by the averages of all

$$p^{\alpha}_{i,j} = \langle\alpha|i\rangle\langle j|\alpha\rangle \tag{7}$$

where i and j are nearest neighbours. i and j are restricted to be either s-type or p-type atomic orbitals, depending on the type of bond order to be calculated. A factor of minus one has been included in the definition of the p_{pp} bond order, so the bond order between bonds of p-type orbitals becomes positive if it is ppσ-bonding. At the top of the VB, the eigenfunctions of the system are almost p-like, because q_s is small there.

To interpret the localization phenomena at the band edges, we have to take into account the following effects. (i) In general, p states are believed to favour localization because of their directional properties. (ii) From the work of Gibbons *et al* (1988) it is known that localization is enhanced by an antibonding character of the states. From the population analysis we derive that at the top of the VB the states have ppσ-bonding character. At the bottom of the CB, on the other hand the eigenfunctions consist of s-type and p-type orbitals in a comparable amount. This alone would suggest a stronger localization at the top of the VB. However, at the bottom of the CB states are ss-antibonding and ppσ-non-bonding, so localization due to disorder should be enhanced. Thus not only the orbital character of eigenfunctions alone, but also the character of bonds is important for the origin of electron localization.

As the inner-band localization is a weak one, its origin cannot be easily deduced. The population analysis for a-C ($p = 0.1$, $1/r^2$-scaling) is plotted in figure 6. For energies below the interval containing localized states in the VB, eigenstates are of s-type and have a bonding character. For higher energies, ppσ-bonding dominates. Both effects lead to an effective suppression of weak localization outside the interval shaded in figure 4 and indicated again in figure 6. Localized eigenfunctions are non-bonding on the average. For these, the orbital character quickly changes from s- to p-type. A similar change from s- to p-type character can be observed in the CB interval consisting of localized states. There, eigenfunctions are both ss- and ppσ-antibonding. For higher energies, the ppσ-antibonding character becomes weaker. No hints for the origin of the extended behaviour of the eigenfunctions to the left of the localized interval in the CB can be obtained from the population analysis.

4. Conclusions

We have performed a numerical study of localization properties on continuous random networks as models of amorphous carbon, silicon and germanium. The geometry of the models is based on the diamond lattice; disorder has been introduced by creating vacancies and rearranging bonds. The network has been relaxed by a Monte Carlo procedure. Nearest neighbour tight-binding Hamiltonians have been used to calculate the electronic structure. Localization properties have been obtained by the TEL method.

Localization properties significantly depend on the degree of disorder, the element and the Hamiltonian used. For Hamiltonians with matrix elements depending on interatomic distance, localization at the bottom of the conduction band is stronger than localization at the top of the valence band for small degrees of disorder. For

larger degrees of disorder, the gap at E_F closes, the gap states show a transition from localized to extended states with further increasing disorder and increasing density of states. The phenomenon of weak inner-band localization is observed for several models. The origin of localization properties is discussed in the frame of population analysis.

Acknowledgments

We thank Dr L Schweitzer (PTB Braunschweig) and Dr D E Logan (Oxford) for fruitful discussions. Financial support from the Deutsche Forschungsgemeinschaft (DFG) and partial support from the Fonds der Chemischen Industrie is gratefully acknowledged. We thank the computing centre of the TU Braunschweig, where the calculations have been performed on an IBM 3090/600 computer.

References

Abrahams E, Anderson P W, Licciardello D C and Ramakrishnan T V 1979 *Phys. Rev. Lett.* **42** 673
Agrawal B K, Agrawal S, Yadav P S and Negi J S 1990 *J. Phys.: Condens. Matter* **2** 6519
Anderson P W 1958 *Phys. Rev.* **109** 1492
Biswas R, Wang C Z, Chan C T, Ho K M and Soukoulis C M 1989 *Phys. Rev. Lett.* **63** 1419
Biswas R, Grest G S and Soukoulis C M 1987 *Phys. Rev.* B **36** 7437
Chadi DJ and Cohen M L 1975 *Phys. Status Solidi* b **68** 405
Connel G A N and Temkin J R 1974 *Phys. Rev.* B **9** 5323
Cullum J K and Willoughby R K 1985 *Lanczos Algorithms for Large Symmetric Eigenvalue Problems, Vol. I. Theory, Vol. II. Programs* (Boston, MA: Birkhäuser)
Dean P and Bell R J 1970 *Discuss. Faraday Soc.* **50** 55
Duffy M G, Boudreaux D S and Polk D E 1974 *J. Non-Cryst. Solids* **15** 435
Edwards J T and Thouless D J 1972 *J. Phys. C: Solid State Phys.* **5** 807
Gibbons M K, Logan D E and Madden P E 1988 *Phys. Rev.* B **38** 7292
Harrison W A 1980 *Electronic Structure and the Properties of Solids* (San Francisco: Freeman)
Henderson D and Herman F 1972 *J. Non-Cryst. Solids* **8–10** 359
Hickey B J and Morgan G J 1986 *J. Phys. C: Solid State Phys.* **19** 6195
Keating P W 1966 *Phys. Rev.* **145** 637
Koslowski Th and von Niessen W 1992 *J. Phys.: Condens. Matter* **4** 1093
Lanczos C 1950 *J. Res. NBS* B **45** 225
Licciardello D C and Thouless D J 1975 *J. Phys. C: Solid State Phys.* **8** 4157
—— 1978 *J. Phys. C: Solid State Phys.* **11** 925
Mott N F and Davis E 1971 *Electronic Processes in Non-Crystalline Solids* (London: Oxford University Press)
Mulliken R S 1955 *J. Chem. Phys.* **23** 1833
Nichols C S and Winer K 1988 *Phys. Rev.* B **38** 9850
Polk D E 1971 *J. Non-Cryst. Solids* **5** 365
Wooten F, Winer K and Weaire D 1985 *Phys. Rev. Lett.* **54** 1392
Ziman J M 1969 *J. Phys. C: Solid State Phys.* **2** 1230